ELSEVIER

Biochimica et Biophysica Acta 1460 (2000) 27–38

BIOCHIMICA ET BIOPHYSICA ACTA
BBA

www.elsevier.com/locate/bba

Review

Atomic force microscopy of native purple membrane

Daniel J. Müller [a,b,*], J. Bernard Heymann [a], Filipp Oesterhelt [c], Clemens Möller [a,d], Hermann Gaub [c], Georg Büldt [d], Andreas Engel [a]

[a] *M.E. Müller-Institute for Structural Biology, Biozentrum, University of Basel, Klingelbergstr. 70, CH-4056 Basel, Switzerland*
[b] *Max-Planck-Insitute of Molecular Cell Biology and Genetics, Pfotenhauerstr. 108, D-01307 Dresden, Germany*
[c] *CeNS, Ludwig-Maximillians Universität München, Amalienstrasse 54, D-80799 München, Germany*
[d] *IBI-2: Structural Biology, Forschungszentrum Jülich, D-52425 Jülich, Germany*

Received 24 March 2000; accepted 24 March 2000

Abstract

Atomic force microscopy (AFM) allows the observation of surface structures of purple membrane (PM) in buffer solution with subnanometer resolution. This offers the possibility to classify the major conformations of the native bacteriorhodopsin (BR) surfaces and to map the variability of individual polypeptide loops connecting transmembrane α-helices of BR. The position, the variability and the flexibility of these loops depend on the packing arrangement of BR molecules in the lipid bilayer with significant differences observed between the trigonal and orthorhombic crystal forms. Cleavage of the Schiff base bond leads to a disassembly of the trigonal PM crystal, which is restored by regenerating the bleached PM. The combination of single molecule AFM imaging and single molecule force-spectroscopy provides an unique insight into the interactions between individual BR molecules and the PM, and between secondary structure elements within BR.

Keywords: Bacteriorhodopsin; *Halobacterium salinarum*; Polypeptide loop; Purple membrane; Structural flexibility; Structural variability; Surface structure; Membrane protein interaction

1. Introduction

The applicability of atomic force microscopy (AFM; [1]) for imaging biological objects in their aqueous environment has been demonstrated shortly after the invention of this technique [2]. Although similar and higher resolution can be obtained by electron microscopy and X-ray crystallography, the excellent signal-to-noise ratio of AFM topographs allows the direct imaging of native proteins [3–8] and their substructures to a resolution of ≈0.5 nm [9]. Thus, imaging of a statistically significant number of single proteins by AFM allows their structural variability to be assessed [10], and multivariate statistical classification to be applied to unravel the principal modes of the protein motion [10]. In addition, AFM enables conformational changes of single proteins and of their assemblies to be observed directly [11–14]. Furthermore, conformational changes can be induced in a controlled manner to identify flexible protein structures [5,8,15].

Abbreviations: AFM, atomic force microscopy; BO, bacterioopsin; BR, bacteriorhodopsin; PM, purple membrane; RMS, root-mean-square

* Corresponding author. Fax: +41-61-267-2109;
E-mail: daniel.mueller@unibas.ch

0005-2728/00/$ – see front matter
PII: S0005-2728(00)00127-4

With the AFM tip, a 'nanotool' is available that allows molecules to be dissected [6] and interactions between single molecules to be detected. In these single molecule force-spectroscopy experiments, the protein complexes are tethered to both support and AFM tip to measure their cohesion when tip and support are moved apart. This technique has been employed to measure forces between pairs of interacting biological molecules [16–21] and forces required for the unfolding of titin domains [22–24]. Protein complexes were imaged before and after the removal of individual subunits using the AFM tip as a nanotool [6]. Based on these results, the single molecule imaging and single molecule force-spectroscopy capabilities of the AFM have been combined to provide novel insights into the inter- and intramolecular interactions of proteins [25,26]. Applied to membrane proteins, these combined techniques allow forces to be measured that anchor the protein in the native membrane, as well as forces required to unfold the tertiary and secondary structure of the protein [26], and the protein to be imaged at subnanometer resolution.

Comparing recent AFM studies of purple membrane (PM), continuous improvement of the AFM imaging of native membrane proteins becomes evident [13,15,27–34]. Here, we review the insights on PM provided by AFM imaging and single-molecule spectroscopy.

2. Identification of the purple membrane surfaces

In our AFM experiments, native PM was allowed to adsorb from buffer solution onto a freshly cleaved mica surface [35]. After being rinsed with the same buffer solution, the PM patches were routinely observed in the fluid cell of the AFM (Fig. 1A). At low magnification, no topographic difference between individual membranes was detected. To distinguish the two surfaces of PM, antibodies directed against the C-terminus located on the cytoplasmic bacteriorhodopsin (BR) surface were injected into the buffer solution [33]. After addition of antibodies, some of the membranes were labeled and had a rough surface (Fig. 1B), whereas others remained as smooth as the membranes shown in Fig. 1A. To further establish the specificity of antibody labeling, the C-terminus was removed by papain digestion of PM. Papain digested PM adsorbed to mica in a similar manner as the native PM, and exhibited the same dimensions and smooth surface texture (Fig. 1C). Consistent with the absence of antibody binding in the dot immunobinding assays no decoration of the digested

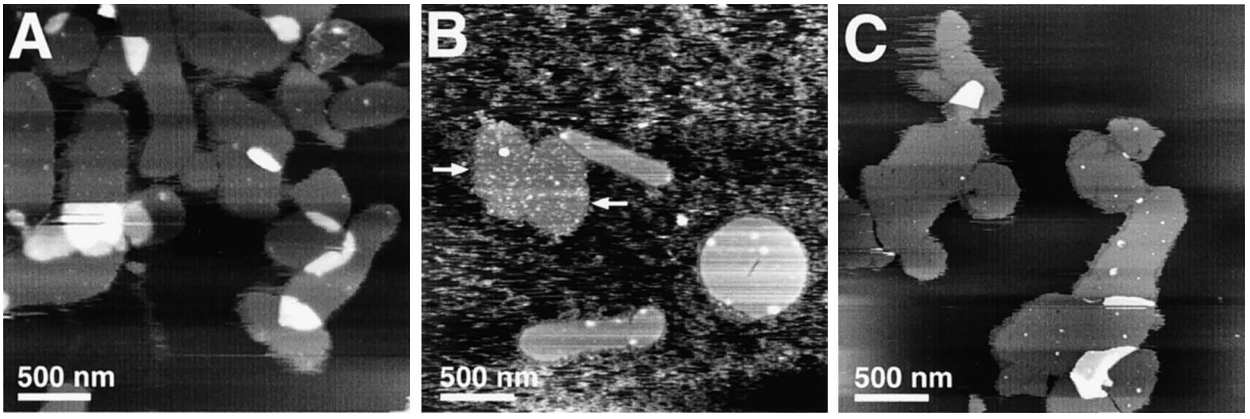

Fig. 1. Immuno atomic force microscopy of purple membrane. (A) Native purple membrane (PM) adsorbed flatly onto freshly cleaved mica. (B) Antibodies were added to the buffer solution after adsorption of the native membranes yielding some densely labeled membranes (*), while others remained unlabeled. The antibodies were directed against the C-terminus of bacteriorhodopsin (BR) located on the cytoplasmic PM surface. Thus, the labeled membranes (arrows) exposed their cytoplasmic surface towards the aqueous solution. Loading force for both images was between 0.1–0.2 nN and the scan frequency was 3.5 Hz. (C) AFM topograph of papain-digested PM leading to the removal of the C-terminus. After incubation with antibodies, digested PM remained untextured even after extending the reaction time for antibody binding from 1 to 24 h at room temperature. Imaging buffer: 150 mM KCl, 10 mM Tris-HCl, pH 8. Forces applied to the AFM tip were between 0.1 and 0.2 nN.

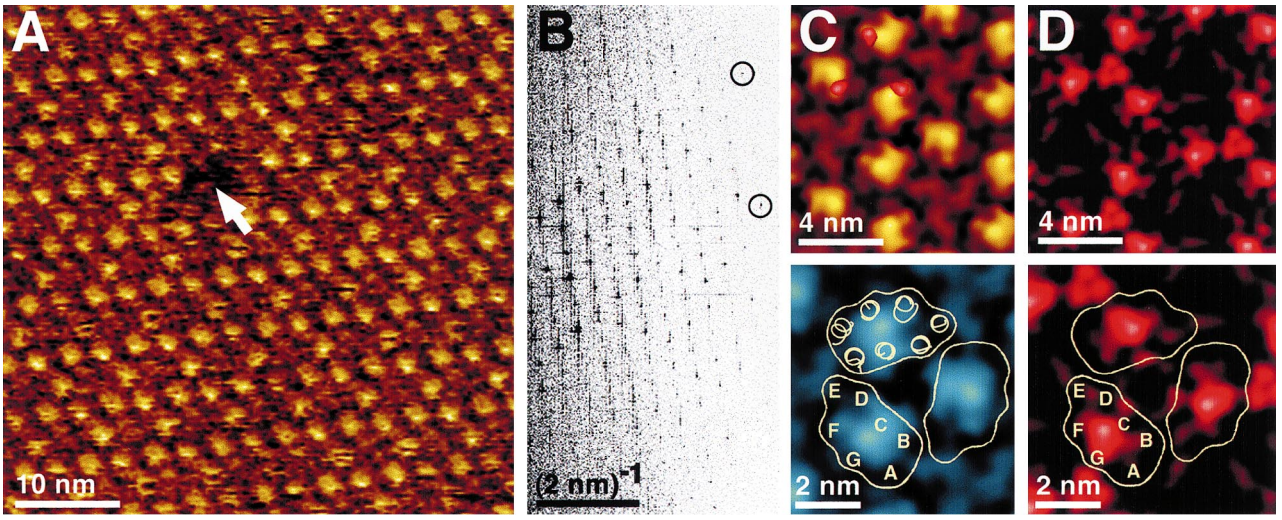

Fig. 2. Extracellular purple membrane surface recorded in buffer solution (A). The PM surface exhibits a defect of the size of a BR trimer (arrow). (B) The power spectrum of A extends to the 11th order indicating a lateral resolution of 0.49 nm. (C) Averaged extracellular surface of the BR trimer (average of 320 unit cells). The correlation average is displayed in perspective view (top, shaded in yellow brown) and in top view (bottom, in blue) with a vertical brightness range of 1 nm and exhibited a 6.1% root-mean-square (RMS) deviation from three-fold symmetry. To assess the flexibility of the different structures, standard deviation (S.D.) maps are calculated (D) and had a range from 0.07 (lipid) to 0.12 nm (region of the FG loop). Surface regions exhibiting an S.D. above 0.1 nm are superimposed in red-to-white shades in top of C. The topograph was recorded in buffer solution (100 mM KCl, 10 mM Tris–HCl, pH 7.8) at a loading force of 100 pN. The outlined BR trimer representing sections close to the extracellular surface of the lipid membrane was obtained after merging five atomic models of BR derived from electron and X-ray crystallography [37].

membranes was observed, even after extending the incubation time with the antibodies from 1 to 24 h [33]. These results indicated that PMs have been specifically labeled by the antibodies directed to the C-terminus when the extracellular surface was in contact with the mica. Thus, those smooth patches of PM not labeled by the antibody, are oriented so that the extracellular surface is on top and imaged by the AFM tip.

3. Extracellular surface of purple membrane

In the low magnification image displayed in Fig. 1B, the labeled PMs were easily distinguished from the unlabeled membranes. A high resolution image of the unlabeled, extracellular surface (Fig. 2A) revealed the arrangement of tripartite protrusions on a trigonal lattice ($a=b=6.2\pm0.2$ nm) exhibiting a maximum height difference to the lipid membrane of 0.53 ± 0.07 nm. The power spectrum (Fig. 2B) exhibited characteristic strong second and third order spots, and extended to the 11th order indicating a lateral resolution of 0.49 nm [13].

Distinct features on the extracellular surface can be assigned to the loops of BR (Fig. 2C). The most prominent protrusion is the β-hairpin in the BC loop connecting the transmembrane α-helices B and C. In the topograph, this protrusion is located between helices C and G. The shoulder near helix A is likely the N-terminus. Loop FG may contribute to the major protrusion, although it does not extend much above the lipid headgroups in the atomic models. However, this area exhibits an enhanced standard deviation (S.D.) of 0.12 nm compared to the background (0.07 nm; Fig. 2D) indicating an increased structural variability and alternative conformations not reflected in the atomic models derived from electron and X-ray crystallography.

4. Cytoplasmic surface of purple membrane

The cytoplasmic BR surface imaged with a force of 100 pN applied to the AFM stylus revealed trimeric structures arranged in a trigonal lattice of 6.2 ± 0.2 nm side length (Fig. 3A, top; [13]. Each subunit in the trimer features a particularly pro-

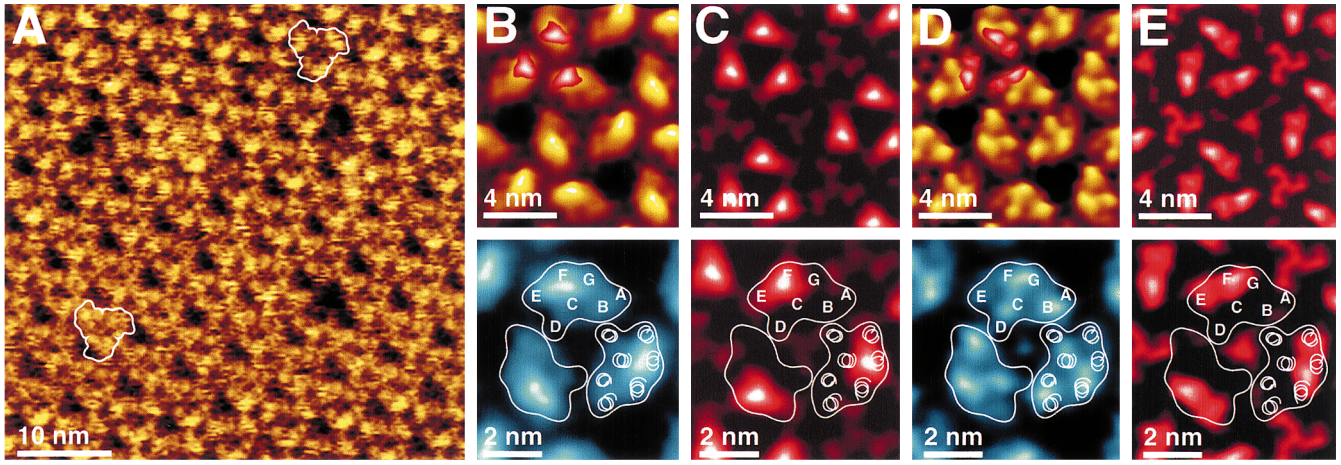

Fig. 3. Force-dependent surface topography of the native cytoplasmic purple membrane surface. (A) At the top of the image, the force applied to the AFM stylus was 100 pN. While scanning the surface line by line, the force was increased until it reached 150 pN at the bottom of the image. This force-induced conformational change of BR was fully reversible [15]. Correlation averages of the cytoplasmic surface recorded at 100 pN (B) and at 200 pN (D). The correlation averages are displayed in perspective view (top, shaded in yellow brown) and in top view (bottom, in blue) with a vertical brightness range of 1 nm and exhibited 9.2% (B) and 14.1% (D) RMS deviations from three-fold symmetry. Structural flexibilities were accessed by S.D. maps (C and E corresponding to B and D, respectively) which had a range from 0.08 (lipid) to 0.19 nm (EF loop region). Surface regions exhibiting an S.D. above 0.12 nm are superimposed in red-to-white shades in the top of B and D. The topograph was recorded in buffer solution (100 mM KCl, 10 mM Tris–HCl, pH 7.8). The outlined BR trimer representing sections close to the cytoplasmic surface of the lipid membrane was obtained after merging six atomic models of BR [37].

nounced protrusion extending 0.83 ± 0.19 nm above the lipid surface. This protrusion is associated with the loop connecting α-helices E and F [15]. Increasing the applied forces to about 200 pN during imaging, the AFM topographs changed significantly. The prominent EF loops were bent away and the shorter loops of the BR monomers were visualized (Fig. 3A bottom and C). This conformational change is fully reversible [15], suggesting that loop EF is a rather flexible element on the cytoplasmic side of the BR molecule. At this force of 200 pN, the maximum height difference between the protein and the lipid membrane was 0.64 ± 0.12 nm. Four distinct protrusions were recognized in almost every monomer, and a further distinct protrusion was present at the center of the trimers. The calculated diffraction pattern of this topograph documents an isotropic resolution out to 0.45 nm (not shown).

While the S.D. of the height measurements was around 0.1 nm for most morphological features of the topography, the EF loop exhibited an S.D. of 0.19 nm (Fig. 3C), consistent with the high temperature factor observed by electron microscopy [36] and the structural variation among the atomic BR models [37]. When the major protrusion representing loop EF had been pushed away by applying a force of 200 pN to the stylus, the cytoplasmic surface of the BR molecule appeared different and exhibited finer details (Fig. 3D).

The protrusion between helices F and G together with the minor elevation between helices E and F likely represents what remained from loop EF and the protruding parts of helices E and F that are compressed by the AFM stylus (Fig. 3D). However, it can not be excluded that the protrusion between helices F and G included a small part of the C-terminal domain. This uncertainty arises because the AFM height signal in this area exhibited a significant standard deviation (Fig. 3E; red shaded in Fig. 3D). The other protrusions in the AFM topograph may be assigned by comparison with the atomic models derived from the BR trimer (see section below). In these models, helix B protrudes out of the bilayer, and helix A ends below the bilayer surface. Therefore, the protrusion close to helix B is likely to represent the short loop connecting helices A and B (Fig. 3D). In addition, the discrete protrusion between helices C and D corresponds to their connecting loop. A further protrusion of 0.2 nm height was present at the three-fold axis of the BR trimer and

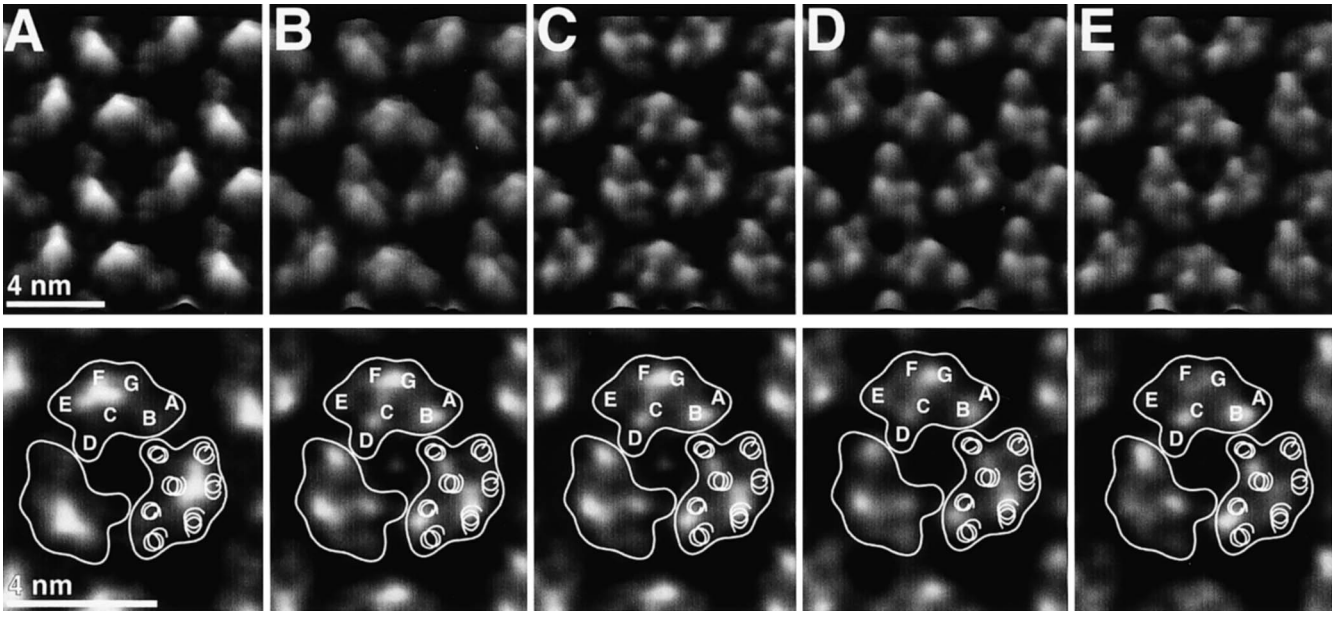

Fig. 4. Structural variability of the native cytoplasmic purple membrane surface. The three-fold symmetrized averages were calculated from unit cells classified by multivariate statistical analysis using the algorithm kindly provided by J.-P. Bretaudiere [74]. (A) PM imaged at slightly enhanced forces of 120 pN (compare to Fig. 3B). Same membrane imaged at an applied force of approximately 150 pN (B). In C, D and E, three conformations of the membrane are imaged at approximately 180 pN. The last three averages differ in their central protrusion. The correlation averages are displayed in perspective view (top) and in top view (bottom) with a vertical brightness range of 1 nm.

probably arises from structured lipid molecules [38–40].

To further analyze the conformations of the cytoplasmic surface, the unit cells of topographs recorded at applied forces of 100 and 200 pN were extracted, aligned with respect to a reference and classified by principal component analysis [41,42]. The three-fold symmetrized averages of the major classes shown in Fig. 4A–E reveal the movement of the flexible structures. The classes A, B, and C, D were closely related to the force gradient. Increasing the force to 120 pN resulted in a slight deformation of the EF loop and enhanced the details of the surrounding protein structure (Fig. 4A; compare with Fig. 3B). Increasing the force to approximately 150 pN further pushed the EF loop away (Fig. 4B), whereas at about 180 pN the conformational change of the loop was complete (Fig. 4C–E). A central protrusion was apparent in some BR trimers when imaged at 180 pN (Fig. 4C,E). Most probably, this protrusion represented lipid-headgroups which was absent or disordered in some BR trimers. Increasing the applied force up to 300 pN resulted in a deformation of the peripheral protrusions of the trimer. The structural information of these areas were lost [10].

5. Surface structures of BR can change upon interactions with adjacent molecules

Recrystallization of BR in the presence of *n*-dodecyl trimethylammonium chloride (DTAC) yielded well-ordered 2D crystals [43] that adsorbed flatly onto freshly cleaved mica. They had sizes of up to 5 μm, and a thickness of 5.8 ± 0.4 nm, which was slightly more than that of the native PM, 5.5 ± 0.4 nm [44]. Topographs of these orthorhombic crystals showed BR dimers assembled into a rectangular lattice with a $p22_12_1$ symmetry and unit cell dimensions of $a = 5.8$ nm, $b = 7.4$ nm (Fig. 5A) [43]. Accordingly, the BR dimers alternately had their cytoplasmic surface or their extracellular surface facing the stylus. The maximum height difference between the protrusions and the bilayer was 0.81 ± 0.09 nm. Surprisingly, it was not possible to induce conformational changes of the EF loops in this BR crystal form.

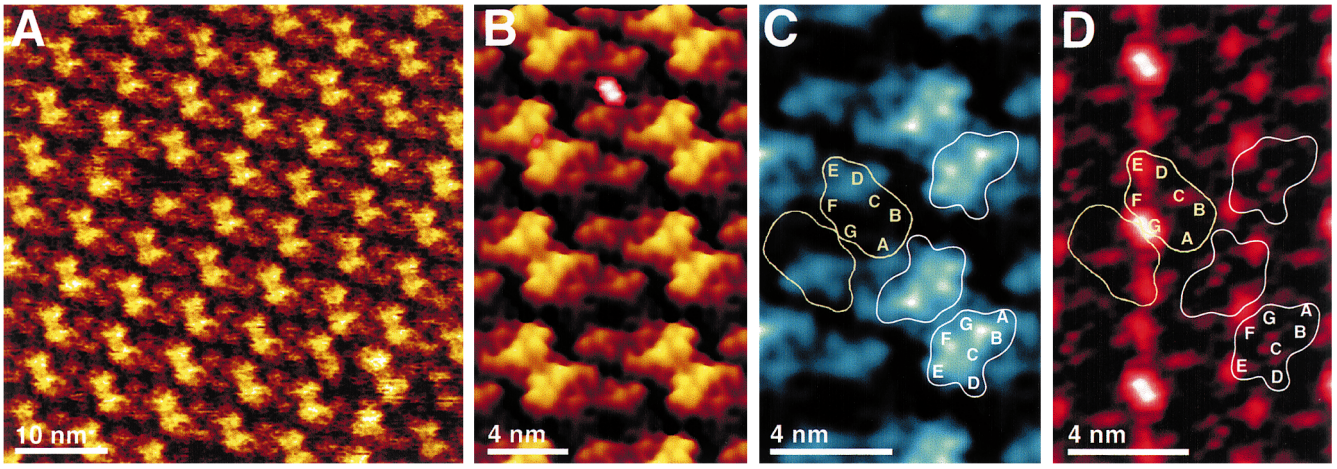

Fig. 5. Native bacteriorhodopsin assembled into an orthorhombic lattice. (A) In this crystal form ($p22_12_1$), the rows of BR dimers alternate, to expose either their cytoplasmic or their extracellular surfaces to the aqueous solution. The correlation averages are displayed (B) in perspective view and (C) in top view with a vertical brightness range of 1 nm. (D) Standard deviation map of C having a vertical brightness range from 0.06 to 0.17 nm. Surface regions exhibiting an S.D. above 0.12 nm are superimposed in red-to-white shades in B. The outlined regions are presented for comparison with the extracellular (yellow outline) and cytoplasmic (white outline) slides of BR as shown in Figs. 2 and 3. The topograph was recorded in buffer solution (100 mM KCl, 10 mM Tris–HCl, pH 7.8) at a loading force of 100 pN.

Increasing the applied force of the stylus resulted in a deformation of the whole protein surface rather than in the bending of a single loop, and reduced the lateral resolution.

The arrangement of the protrusions on the cytoplasmic face of BR was very distinct when AFM topographs of the orthorhombic in vitro assemblies were analyzed (Fig. 5B,C). The protrusion of the AB loop was shifted by 0.3 nm compared to the trigonal unit cell (Fig. 3), now being located between the position of helices A and B (Fig. 5C). The short loop connecting helices C and D was observed as a discrete protrusion in the orthorhombic lattice, close to its position in the trigonal lattice. Remarkably, the EF loop was observed as a bean shaped structure independent of the applied force (Fig. 5C). The triangular protrusion located between helices B and G may result from the C-terminus. None of these structures exhibited significant variabilities, indicating a structural stabilization by the different packing arrangement in the orthorhombic compared to the trigonal lattice. An additional protrusion (Fig. 5C) was observed at the periphery of each BR monomer packed in the orthorhombic lattice, probably representing bound lipid molecules [38–40].

The observed structural changes suggest that the interactions of the cytoplasmic polypeptide loops depend on how the BR molecules associate. In the BR trimer, there is a crevice between helices A and B, and helices E and D of neighboring monomers (Fig. 3C–E; outlined). Lipid molecules in this crevice are stable [36], and stabilize the BR trimer by specific interactions with their lipid and head-group molecules [38–40]. This crevice is not present in the orthorhombic BR assembly and hence, the different molecular interactions probably allow the displacement of the loop connecting helices A and B (Fig. 5C; white contours). From our data, we conclude that in the orthorhombic BR crystals, the interactions between helices F and G of two adjacent BR molecules affected both the structural appearance and increased the rigidity of the EF loop and of the C-terminal region.

On the extracellular surface of BR in the orthorhombic crystal, the most prominent protrusion arising from the β-hairpin is at a different position as observed in the BR trimer (Fig. 2). Compared to the topography of the trigonal crystal, the main protrusion of the hairpin is shifted away from the center of the BR molecule and its height above the bilayer is increased by 0.1 nm. This rather large rearrangement of the BC loop observed in the orthorhombic lattice presumably results from the different crystal contacts and the altered protein and lipid in-

teractions. In contrast, the short loop connecting helices E and D was apparently not influenced by the different packing arrangement. Interestingly, the region between F and G exhibits an enhanced standard deviation in the orthorhombic lattice (0.17 nm, red shaded) and the connecting loop did not make a contribution to the average. Thus, in contrast to the cytoplasmic surface, the crystal contacts along helices F and G did not stabilize the corresponding extracellular loops. A protrusion (Fig. 5) was found to occur in the crevice between two BR monomers. This protrusion corresponds to the position of the triglycoside head-groups of lipids which also occurred ordered in the center of the BR trimer (Fig. 3D) [45].

6. Implications of combining AFM data with the atomic models of BR

Information about the surfaces of BR have been derived from electron crystallography [36,40], and X-ray diffraction [38,45–47] at high resolution, and AFM at medium resolution (Figs. 2–5). This provided an excellent opportunity to assess the quality of the AFM topographs of the PM, and to understand the implications of combining AFM data with the other structure determination methods. Six BR atomic models were combined and compared with the AFM data to determine the value and reliability of each source of information [37].

Fig. 6 shows one atomic model suspended within an envelope of the PM reconstructed from the AFM data. The ribbon diagram is color coded according to the coordinate variance between the different atomic models, while the surfaces are mapped with the AFM S.D. images. There is an excellent correspondence between the surface loops of the BR model and the AFM envelope. S.D. maps of the height measured by AFM corresponds well with the relative distribution of B-factors of the atomic models, as well as the coordinate variance between the models. This agrees with the notion that the major difference between the various structural studies lies in the surfaces.

In the case of AFM, a 2D crystal of BR close to its native state is imaged, allowing surface loops the maximum possible freedom of conformation. In electron crystallography, the loops are also more exposed on the 2D crystal surface, although embedding it in a cryoprotectant and freezing it limits the loop dynamics to some extent. In X-ray crystallography, the surface loops are better resolved, but they are often involved in 3D crystal contacts and may not represent their true conformational state and variation in vivo. Specifically, the EF loop appears to adopt different conformations in the 2D assembly of BR molecules of PM, while it has less conformational freedom in the 3D crystals. This agrees with electron paramagnetic resonance (EPR) spectroscopy of spin-labeled cysteine mutants showing a high mobility of residues S158–P165 in the EF loop [48]. In contrast to electron and X-ray crystallography methods, the AFM can be used to image surface structures of BR in buffer solution and at room temperature, similar to their physiological environment. Under these conditions, the S.D. maps of BR show a higher peak for the longer and less structured loop

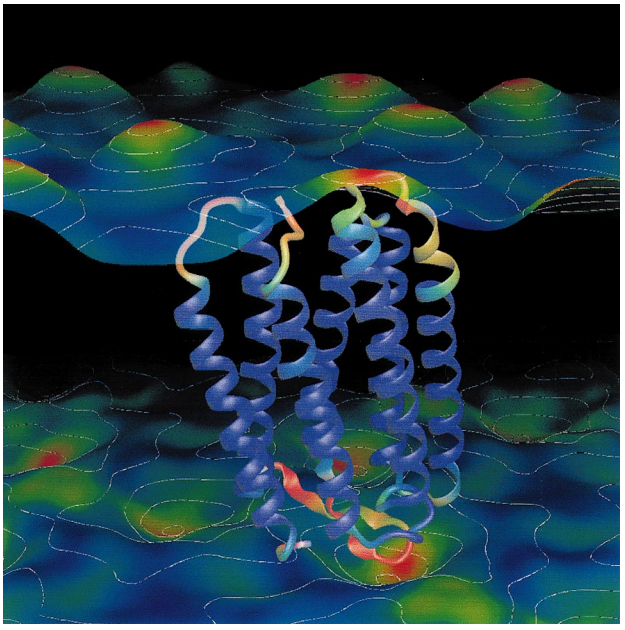

Fig. 6. Mapping the structural variance of bacteriorhodopsin on the atomic model and the AFM envelope. The atomic model is an average of six models derived from electron and X-ray crystallography, with the coordinate variance mapped from blue (low variance) to red (high variance). The surfaces are derived from the AFM height images, with the S.D. mapped onto each surface from blue (low S.D.) to red (high S.D.). The minimum separation between the surfaces is ~4 nm. Calculations are as given in [37].

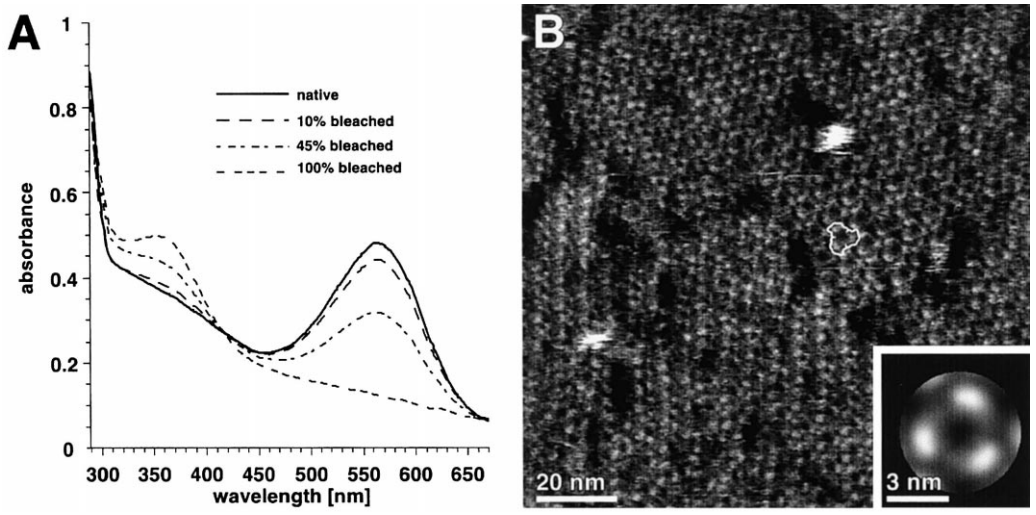

Fig. 7. Structural changes of photobleached purple membrane. (A) Absorption spectra of wild-type PM (solid line) and of PM photobleached in hydroxylamine to 10, 45 and 100% (dashed lines). (B) Topograph of the cytoplasmic surface of purple membrane photobleached to 100%. A single BR trimer is outlined in the raw data. The inset represents the correlation average of the BR trimer. The image was recorded in buffer solution (150 mM KCl, 10 mM Tris–HCl, pH 7.8) at a loading force of 100 pN. Vertical full gray level range, 1.2 nm.

EF, compared to the BC loop which forms a short β-sheet.

The N- and C-termini of BR are not resolved in any of the structural studies. This suggests high flexibility, and the atomic models and AFM data indicate that the N-terminus up to R7, and most of the C-terminus are completely unstructured and averaged out.

7. Structural changes of photobleached purple membrane

The Schiff base of BR reacts with reagents such as hydroxylamine under illumination with light [49]. This chemical reaction results in the breakage of the Schiff base bond between the BR and the retinal yielding the apoprotein bacterioopsin (BO) and retinaloxime. Consequently, the absorption maximum of PM at 568 nm diminishes and an absorption maximum of retinaloxime at about 366 nm is observed [49]. These spectral changes depend upon the illumination time and reflect the photobleaching process of PM (Fig. 7A). The loss of the Schiff base bond leads to structural changes in the apoprotein [50,51]. As observed using AFM, the process of photobleaching was associated with the disassembly of the purple membrane crystal into smaller crystals. As a consequence, entirely bleached PM lost most of its crystalline nature (Fig. 7B). High resolution topographs showed separation of bacteriorhodopsin trimers, first along same lattice lines and later all over the membrane. Furthermore, the topographs showed that the BO molecules remained stably assembled into trimers during the entire photobleaching process. Regeneration of the photobleached membranes into fully active PM resulted in the reassembly of the BR trimers into a trigonal crystal. The regenerated membranes exhibited similar diameters, thicknesses and crystallinity as native PM [52].

From these results, it can be concluded, that the transformation of BR into BO changes the interactions between the trimers. Such interactions might result from changes in the tertiary structure of the protein. Since the BR trimer remains stable during the entire course of photobleaching, it might be concluded that major structural changes occur at the rim of the trimer where it interacts with adjacent lipids. These interfaces are lined by helices A, E and F, and by helix G to which the retinal is bond. Cleavage of the Schiff base is followed by a reversible change of these interfaces and a disassembly of the two-dimensional PM crystal.

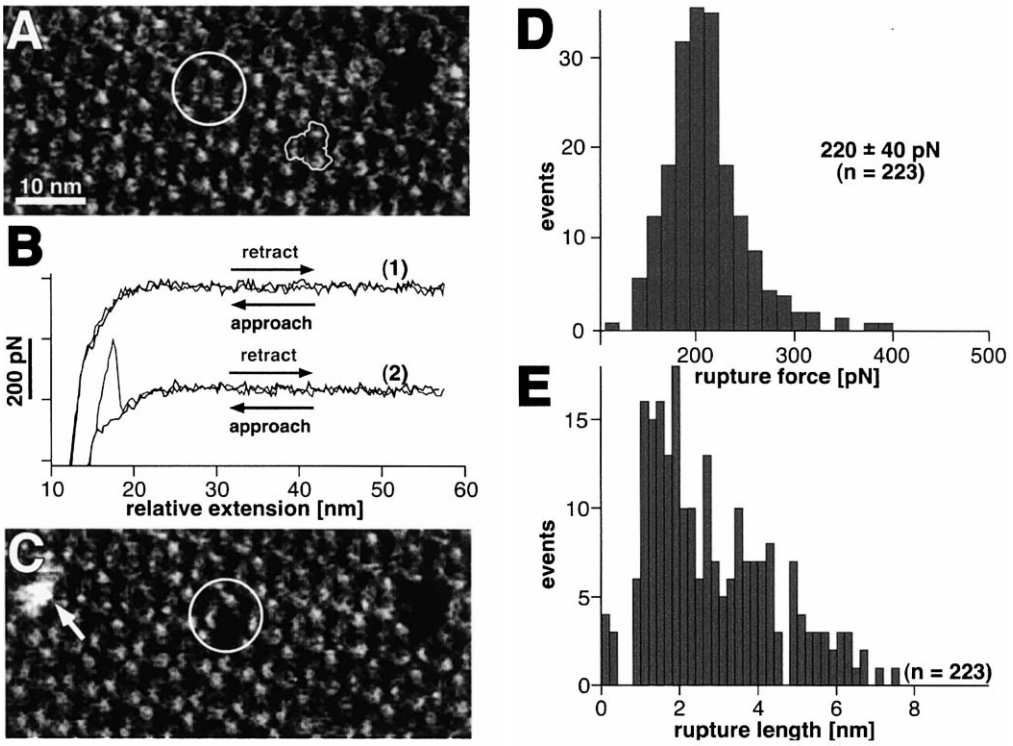

Fig. 8. Extracting individual bacteriorhodopsins from native purple membrane. (A) AFM topograph of the cytoplasmic surface of PM recorded in buffer solution. The BR molecules forming trimers (outlined trimer) are clearly visible. (B) Most of the extension curves recorded on the cytoplasmic surface were unspectacular (1). However, 10% of the other extension curves showed one adhesion peak at a separation of several nm from the PM surface (2). The adhesion force of the peak shown in (2) was about 220 pN. (C) The topograph of the same surface imaged after recording the adhesive force peak showed one BR monomer missing (outlined circle). After extraction of the BR from the PM, a protrusion of about the size of an individual BR molecule was observed to be adsorbed onto the membrane surface (arrow). The missing trimer at the upper right was taken to align the topographs. Full gray level range of topographs, 1.5 nm. (D) Histogram of the rupture forces required to pull an individual BR from the PM. The average adhesion force was 220 ± 40 pN ($n = 223$). (E) Histogram of the pulling lengths until the BR molecules were extracted from the membrane.

8. How strong is bacteriorhodopsin anchored into the purple membrane?

Membrane proteins acquire their unique functions through specific folding of their polypeptide chains and specific interactions with the lipid bilayer and adjacent proteins. Their stability or resistance to unfolding, which goes hand in hand with their anchoring into the hydrophobic core of the membrane, have usually been investigated by thermal or chemical denaturation [53,54]. Most membrane proteins, however, are designed to remain stably embedded in the lipid leaflets rather than to withstand heat or a harsh change in their chemical environment. As described by the fluid mosaic model [55], the membrane protein and a few tightly bound lipids can diffuse within the bilayer plane without significant resistance while the protein is anchored vertically to the membrane plane. It is expected that the stability of membrane proteins involves interactions with the lipid bilayer as well as intra- and intermolecular interactions [53]. Thus, it is important to directly measure the forces that anchor membrane proteins in the membrane.

To answer this pertinent question in membrane biology, atomic force microscopy (AFM; [1,2]) and single-molecule force spectroscopy [16,17,20–23,56–59] were combined. After imaging PM (Fig. 8A), the AFM stylus was pushed towards the PM surface exerting a force of about 1 nN, thereby allowing individual BR to adsorb onto the stylus [22,25,35,57]. When the two surfaces were separated, extension curves like the ones shown in Fig. 8B were recorded. In most of the curves, no adhesive force was ob-

served (Fig. 8B; upper curve). However, in ≈10% of the curves an adhesive force indicated that molecular structures bridged the stylus and the protein surface (Fig. 8B; (lower curve)). When re-imaged after recording such force–extension curves the PM surface appeared changed and an individual BR molecule was found to be missed (Fig. 8C). This indicated that a single BR molecule adhered to the AFM stylus and was extracted upon separation of the stylus from the membrane. Interestingly, it was observed that the extracted BR molecule adsorbed on the PM close to the area where the removal took place. Repeating the experiment more than 220 times showed that an individual adhesion peak resulted in the removal of an individual membrane protein and that the adhesion had an average force of about 220 ± 40 pN (Fig. 8D; pulling speed, 20 nm/s). In most extension traces from the PM surface (≈95%), the adhesion force was already evident at the membrane surface. The average stretching until rupture between the protein, adsorbed to the AFM stylus, and the membrane, was 2.8 ± 1.6 nm (Fig. 8D). This stretching length agrees favorably with the thickness of the hydrophobic region within the PM, ≈3–3.5 nm [36,45,46,60–62], anchoring the BR molecules. From these findings we conclude that in this kind of rupture, the entire BR molecule was extracted from the PM in one single step. As recently reported by the work of Oesterhelt et al. [26] using slightly modified conditions, the AFM tip can be attached to the C-terminus to unfold the entire BR. The unfolding of BR helices was similar as observed for the unzipping of bacterial pores of the bacterial surface layer of *Deinoccocus radiodurans* [25]. While unfolding the BR, interactions between transmembrane α-helices were detected. Most interestingly, the force spectra of single BR molecules revealed different pathways of unfolding.

9. Conclusions and future perspectives

The AFM topographs of BR surfaces recorded in buffer solution at room temperature clearly show the conformations of the polypeptide loops. The signal-to-noise ratio of the topographs allows the observation of details on single BR molecules and their major conformations can be classified. To assess the structural variability of the surface structures S.D. maps can be calculated, revealing the elasticity of single loops. These important improvements of the AFM application and data analysis provide evidence that the AFM not only fulfills the prerequisites to directly monitor function related conformational changes of biological macromolecules [2,12,14,63], but can also characterize dynamic aspects of protein structures, such as their flexibility and variability. In the case of BR, we have shown that protrusions representing single polypeptide loops exposed to the aqueous solution, can change their structure, variability and flexibility upon interactions occurring within the membrane composed of proteins and lipids.

Good correspondence of loop structures between the different structure determination techniques have been shown. In addition, each technique provides similar, but also complementary information. X-ray crystallography is the premier technique for atomic resolution, while electron crystallography examines the specimen in a more native-like environment at near-atomic resolution. AFM offers an even better assay of surface structure and variation at submolecular resolution under physiological conditions. The combination of these techniques thus represents a complete structural analysis of the specimen.

The flexibility in the loop EF may be important for function, as the observed movement of helix F during the photocycle [64–68] would require a conformational change in loop EF. Loops AB and BC are much more stable than loop EF, and their roles in providing 3D crystal contacts should therefore not be a surprise.

Although the observed structural changes may not significantly influence the proton pumping function of BR [43], they would be of crucial importance for transmembrane proteins whose surface regions are known to interact with other proteins. In particular, such receptor proteins exhibiting seven transmembrane α-helices which belong to the G-protein-coupled family [69–72] will be an important focus in further investigations [73].

Acknowledgements

This work was supported by the Swiss National Foundation for Scientific Research (NFP).

References

[1] G. Binnig, C.F. Quate, C. Gerber, Phys. Rev. Lett. 56 (1986) 930–933.
[2] B. Drake, C.B. Prater, A.L. Weisenhorn, S.A.C. Gould, T.R. Albrecht, C.F. Quate, D.S. Cannell, H.G. Hansma, P.K. Hansma, Science 243 (1989) 1586–1588.
[3] F.A. Schabert, C. Henn, A. Engel, Science 268 (1995) 92–94.
[4] J. Mou, D.M. Czajkowsky, S. Sheng, R. Ho, Z. Shao, FEBS Lett. 381 (1996) 161–164.
[5] D.J. Müller, A. Engel, J. Carrascosa, M. Veléz, EMBO J. 16 (1997) 101–107.
[6] D. Fotiadis, D.J. Müller, G. Tsiotis, L. Hasler, P. Tittmann, T. Mini, P. Jenö, H. Gross, A. Engel, J. Mol. Biol. 283 (1998) 83–94.
[7] D.M. Czajkowsky, S. Sheng, Z. Shao, J. Mol. Biol. 276 (1998) 325–330.
[8] S. Scheuring, P. Ringler, M. Borgina, H. Stahlberg, D.J. Müller, P. Agre, A. Engel, EMBO J. 18 (1999) 4981–4987.
[9] D.J. Müller, D. Fotiadis, S. Scheuring, S.A. Müller, A. Engel, Biophys. J. 76 (1999) 1101–1111.
[10] D.J. Müller, D. Fotiadis, A. Engel, FEBS Lett. 430 (1998) 105–111.
[11] D.J. Müller, W. Baumeister, A. Engel, J. Bacteriol. 178 (1996) 3025–3030.
[12] D.J. Müller, C.-A. Schoenenberger, F. Schabert, A. Engel, J. Struct. Biol. 119 (1997) 149–157.
[13] D.J. Müller, H.-J. Sass, S. Müller, G. Büldt, A. Engel, J. Mol. Biol. 285 (1999) 1903–1909.
[14] D.J. Müller, A. Engel, J. Mol. Biol. 285 (1999) 1347–1351.
[15] D.J. Müller, G. Büldt, A. Engel, J. Mol. Biol. 249 (1995) 239–243.
[16] E.-L. Florin, V.T. Moy, H.E. Gaub, Science 264 (1994) 415–417.
[17] G.U. Lee, L.A. Chrisey, R.J. Colton, Science 266 (1994) 771–773.
[18] G.U. Lee, D.A. Kidwell, R.J. Colton, Langmuir 10 (1994) 354–357.
[19] V.T. Moy, E.-L. Florin, H.E. Gaub, Coll. Surf. A93 (1994) 343–348.
[20] U. Dammer, O. Popescu, P. Wagner, D. Anselmetti, H.J. Güntherodt, G.N. Misevic, Science 267 (1995) 1173–1175.
[21] U. Dammer, M. Hegner, D. Anselmetti, P. Wagner, M. Dreier, W. Huber, H.J. Güntherodt, Biophys. J. 70 (1996) 2437–2441.
[22] M. Rief, M. Gautel, F. Oesterhelt, J.M. Fernandez, H.E. Gaub, Science 276 (1997) 1109–1112.
[23] A.F. Oberhauser, P.E. Marszalek, H.P. Erickson, J.M. Fernandez, Nature 393 (1998) 181–185.
[24] M. Carrion-Vazquez, A.F. Oberhauser, S.B. Fowler, P.E. Marszalek, S.E. Broedel, J. Clarke, J.M. Fernandez, Proc. Natl. Acad. Sci. USA 96 (1999) 3694–3699.
[25] D.J. Müller, W. Baumeister, A. Engel, Proc. Natl. Acad. Sci. USA 96 (1999) 13170–13174.
[26] F. Oesterhelt, D. Oesterhelt, M. Pfeiffer, A. Engel, H. Gaub, D.J. Müller, Science 288 (2000) 143–146.
[27] D.L. Worcester, R.G. Miller, P.J. Bryant, J. Microsc. 152 (1988) 817–821.
[28] D.L. Worcester, H.S. Kim, R.G. Miller, P.J. Bryant, J. Vac. Sci. Technol. A8 (1990) 403–405.
[29] H.-J. Butt, K.H. Downing, P.K. Hansma, Biophys. J. 58 (1990) 1473–1480.
[30] H.-J. Butt, C.B. Prater, P.K. Hansma, J. Vac. Sci. Technol. B9 (1991) 1193–1197.
[31] H.-J. Butt, R. Guckenberger, J.P. Rabe, Ultramicroscopy 46 (1992) 375–393.
[32] D.J. Müller, F.A. Schabert, G. Büldt, A. Engel, Biophys. J. 68 (1995) 1681–1686.
[33] D.J. Müller, C.A. Schoenenberger, G. Büldt, A. Engel, Biophys. J. 70 (1996) 1796–1802.
[34] C. Möller, M. Allen, V. Elings, A. Engel, D.J. Müller, Biophys. J. 77 (1999) 1050–1058.
[35] D.J. Müller, M. Amrein, A. Engel, J. Struct. Biol. 119 (1997) 172–188.
[36] N. Grigorieff, T.A. Ceska, K.H. Downing, J.M. Baldwin, R. Henderson, J. Mol. Biol. 259 (1996) 393–421.
[37] J.B. Heymann, D.J. Müller, E. Landau, J. Rosenbusch, E. Pebay-Peroulla, G. Büldt, A. Engel, J. Struct. Biol. 128 (1999) 243–249.
[38] H. Belrhali, P. Nollert, A. Royant, C. Menzel, J.P. Rosenbusch, E.M. Landau, E. Pebay-Peyroula, Struct. Fold. Des. 7 (1999) 909–917.
[39] H. Luecke, B. Schobert, H.T. Richter, J.-P. Cartailler, J.K. Lanyi, J. Mol. Biol. 291 (1999) 899–911.
[40] K. Mitsuoka, T. Hirai, K. Murata, A. Miyazawa, A. Kidera, Y. Kimura, Y. Fujiyoshi, J. Mol. Biol. 286 (1999) 861–882.
[41] M. van Heel, Ultramicroscopy 13 (1984) 165–184.
[42] J. Frank, J.-P. Bretaudiere, J.-M. Carazo, A. Veschoor, T. Wagenknecht, J. Microsc. 150 (1987) 99–115.
[43] H. Michel, D. Oesterhelt, R. Henderson, Proc. Natl. Acad. Sci. USA 77 (1980) 338–342.
[44] D.J. Müller, A. Engel, Biophys. J. 73 (1997) 1633–1644.
[45] L.-O. Essen, R. Siegert, W.D. Lehmann, D. Oesterhelt, Proc. Natl. Acad. Sci. USA 95 (1998) 11673–11678.
[46] H. Luecke, H.-T. Richter, J.K. Lanyi, Science 280 (1998) 1934–1937.
[47] H. Sato, K. Takeda, K. Tani, T. Hino, T. Okada, M. Nakasako, N. Kamiya, T. Kouyama, Acta Crystallogr. D Biol. Crystallogr. 55 (1999) 1251–1256.
[48] M. Pfeiffer, T. Rink, K. Gerwert, D. Oesterhelt, H.-J. Seinhoff, J. Mol. Biol. 287 (1999) 163–171.
[49] D. Oesterhelt, L. Schuhmann, H. Gruber, FEBS Lett. 44 (1974) 257–261.
[50] B. Becher, J.Y. Cassim, Biophys. J. 19 (1977) 285–297.
[51] P.-J. Bauer, N.A. Dencher, M.P. Heyn, Biophys. Struct. Mechanism 2 (1976) 79–92.
[52] C. Möller, G. Büldt, N. Dencher, A. Engel, D.J. Müller, submitted.
[53] T. Haltia, E. Freire, Biochim. Biophys. Acta 1228 (1995) 1–27.
[54] S.H. White, W.C. Wimley, Annu. Rev. Biophys. Biomol. Struct. 28 (1999) 319–365.

[55] S.J. Singer, G.L. Nicolson, Science 175 (1972) 720–731.
[56] R. Merkel, P. Nassoy, A. Leung, K. Ritchie, E. Evans, Nature 397 (1999) 50–53.
[57] M. Rief, F. Oesterhelt, B. Heymann, H.E. Gaub, Science 275 (1997) 1295–1298.
[58] S.B. Smith, Y. Cui, C. Bustamante, Science 271 (1996) 795–798.
[59] P. Hinterdorfer, W. Baumgartner, H.J. Gruber, K. Schilcher, H. Schindler, Proc. Natl. Acad. Sci. USA 93 (1996) 3477–3481.
[60] R. Henderson, J.M. Baldwin, T.A. Ceska, F. Zemlin, E. Beckman, K.H. Downing, J. Mol. Biol. 213 (1990) 899–929.
[61] Y. Kimura, D.G. Vassylev, A. Miyazawa, A. Kidera, M. Matsushima, K. Mitsuoka, K. Murata, T. Hirai, Y. Fujiyoshi, Nature 389 (1997) 206–211.
[62] E. Pebay-Peyroula, G. Rummel, J.P. Rosenbusch, E.M. Landau, Science 277 (1997) 1676–1681.
[63] A. Engel, Y. Lyubchenko, D.J. Müller, Trends Cell Biol. 9 (1999) 77–80.
[64] N.A. Dencher, D. Dresselhaus, G. Zaccai, G. Büldt, Proc. Natl. Acad. Sci. USA 86 (1989) 7876–7879.
[65] M.H.J. Koch, N.A. Dencher, D. Oesterhelt, H.-J. Plöhn, G. Rapp, G. Büldt, EMBO J. 10 (1991) 521–526.
[66] S. Subramaniam, M. Gerstein, D. Oesterhelt, R. Henderson, EMBO J. 12 (1993) 1–8.
[67] S. Subramaniam, M. Lindahl, P. Bullough, A.R. Faruqi, J. Tittor, D. Oesterhelt, L. Brown, J. Lanyi, R. Henderson, J. Mol. Biol. 287 (1999) 145–161.
[68] J. Vonck, Biochemistry 35 (1996) 5870–5878.
[69] R. Henderson, F.R.S. Shertler, G.F.X. Shertler, Phil. Trans. R. Soc. Lond. B 326 (1990) 379–389.
[70] P.A. Hargrave, Curr. Opin. Struct. Biol. 1 (1991) 575–581.
[71] J.M. Baldwin, EMBO J. 12 (1993) 1693–1703.
[72] E.J.M. Helmreich, K.-P. Hofmann, Biochim. Biophys. Acta 1286 (1996) 285–322.
[73] J.B. Heymann, M. Pfeiffer, V. Hildebrandt, D. Fotiadis, B. de Groot, R. Kabak, A. Engel, D. Oesterhelt, D.J. Müller, Structure (2000) in press.
[74] J.-P. Bretaudiere, J. Frank, J. Microsc. 144 (1986) 1–14.